



## Experimental and numerical investigations of CFRP reinforced masonry beams performance under bending loads

Mahmoud Zaghlal

Zagazig University, Egypt

eng\_m\_ز@yahoo.com, <http://orcid.org/0000-0001-2345-6789>

Alaa El-Sisi

Southern Illinois University Edwardsville, USA; on research leave from Zagazig University, Egypt

AElsisi@siue.edu, <http://orcid.org/0000-0002-2345-6790>

Mohamed Husain, Samar Samy

Zagazig University, Egypt

mo\_husain2000@yahoo.com, <http://orcid.org/0000-0002-2345-6791>

samarsamy77777@gmail.com, <http://orcid.org/0000-0003-2345-6792>

**ABSTRACT.** In this paper, an experimental and numerical study was achieved to investigate the behavior of masonry beams internally reinforced using carbon fiber-reinforced polymer (CFRP) and hybrid steel/CFRP reinforcements. Three beams were built using concrete bricks and grout mortar. The brick was designed with two holes that were filled with grout before placing the rebar inside. One beam was built without shear reinforcement, and the other two were with shear reinforcement. Material characterization tests were performed to evaluate the compressive strength of the brick and the masonry cube and the flexural strength of the masonry prism. The masonry cubes were prepared and tested to evaluate their equivalent mechanical properties. The beams were tested in three-point bending with an effective simply supported span of 840 mm where the load deformations and failure loads were monitored. Finite element models were built using ANSYS and validated with experimental results. Additional beam models were analyzed to study the effect of shear reinforcement spacing from 0.78d to 0.39d and more hybrid reinforcement configurations. Results showed that using equivalent material properties in numerical modeling instead of modeling bricks and mortar was acceptable. In addition, using shear reinforcement with a spacing of 0.78 d didn't enhance the shear behavior of the spacing. Finally, the hybrid steel/CFRP-reinforced beam with shear



**Citation:** Zaglal, M., El-Sisi, A., Husain, M., Samy, S., Experimental and numerical investigations of CFRP reinforced masonry beams performance under bending loads, 66 (2023) 1-16.

**Received:** 01.02.2023

**Accepted:** 03.07.2023

**Online first:** 09.07.2023

**Published:** 01.10.2023

**Copyright:** © 2023 This is an open access article under the terms of the CC-BY 4.0, which permits unrestricted use, distribution, and reproduction in any medium, provided the original author and source are credited.



reinforcement achieved the highest capacity compared to the two other beams.

**KEYWORDS.** Experimental, ANSYS, CFRP, Hybrid reinforcement, Static loading, Masonry beams.

## INTRODUCTION

Corrosion is a significant hazard for steel-reinforced concrete structures, being responsible for the deterioration of the physical-mechanical properties of the rebar, particularly in marine environments. Aggressive conditions that feature chlorides, chemicals, and gases can lead to severe damage to metallic reinforcement. To address these issues, new techniques have emerged, including the adoption of alternative non-metallic reinforcement methods. Continuous glass, carbon, basalt, and aramid fibers are the types of fibers used for structural engineering applications. Carbon fiber-reinforced polymer (CFRP) bars have emerged as the preferred choice to improve the structural behavior of masonry due to their environmental sustainability over the past two decades. Compared to metals, CFRP bars exhibit excellent resistance to chemical environments such as acid, alkaline, and saline solutions. Recently, CFRP bars have gained widespread popularity globally due to their effectiveness in retrofitting and strengthening existing structures such as beams, columns, and slab steel. Additionally, CFRP bars possess outstanding structural properties such as high tensile strength, a high strength-to-weight ratio, and non-corrosive, non-magnetic attributes. The strength-to-weight ratio of CFRP bars is 10-15 times higher than that of steel bars [1–10].

Using non-corrosive FRP (fiber-reinforced polymer) bars in such constructions has proven advantageous in overcoming the issue of steel corrosion and effectively enhancing durability [11]. Although research on the behavior of masonry beams reinforced with various types of FRP bars has been limited, researchers have found that the flexural capacity and stiffness of reinforced masonry beams improved significantly as the internal reinforcement ratio increased [12]. Furthermore, the maximum beam capacity of reinforced concrete structural components could be reasonably predicted through the use of reinforced masonry [13]. It was revealed that increased horizontal bed joint reinforcement resulted in enhanced flexure and ultimate deflection [14]. Additionally, the performance of near-surface mounted (NSM) FRP bars with beams and walls has proven to be very effective in improving the flexural strength and failure of masonry beams [11,15]. A study was conducted to examine the flexural behavior of reinforced masonry beams that were internally reinforced with carbon fiber-reinforced polymeric (CFRP) bars and had polyvinyl alcohol (PVA) fibers and polyester fiber bed joints [16]. The study's findings revealed that using engineered cementitious composite (ECC) as a bed joint instead of polyester-ECC and an internal CFRP reinforcement ratio resulted in significant improvements in both load-carrying capacity and ductility [16]. Another study investigated the flexural performance of masonry beams reinforced with CFRP bars using two approaches, pultrusion and hand-layup under four-point bending [17]. The results indicated that the load-carrying capacity of hand-layup CFRP bars had increased by 12 times that of unreinforced masonry beams [17].

The modeling of masonry was used to define its structural behavior or understand its material behavior [18]. Generally, some research concentrated [11,19,20] on two numerical methods of masonry, namely micro-modeling as a separate material and macro-modeling as a composite material, to create homogenization techniques. Tests were conducted on compression and shear wall models made of autoclaved aerated concrete (AAC) masonry units in axial and diagonal compression tests [19]. The results show that the analysis of compression walls can be successfully conducted using both the micro and macro models, while shear walls require a more detailed computational approach [19]. The behavior of a single type of solid, unreinforced masonry shear wall under in-plane loads was also studied [20]. The results show that the micro and macro models employed to evaluate an unreinforced masonry shear wall were similar to the experimental results obtained in the literature [20]. The performance of a reinforced masonry beam subjected to four-point bending, in addition to a full-scale wall confined at three edges and loaded until failure with a distributed out-of-plane pressure, was investigated [11]. The results indicated that the combination of vertical and horizontal ties improved the collapse of masonry beams [11].

To the best of the authors' knowledge, there has been a limited amount of research conducted to investigate the effectiveness of using CFRP bars for internal reinforcement in masonry beams. As a result, there is still much to learn about the behavior of such beams, and the understanding of their performance remains deficient. Therefore, this paper aims to provide an examination of the performance of masonry beams reinforced with CFRP rebars. To maximize the benefits of both experimental and numerical studies, three different tension reinforcement configurations were implemented: pure CFRP



rebar without stirrups, pure CFRP rebar with stirrups, and hybrid CFRP/steel rebar with stirrups. The beams were subjected to a static three-point bending test with careful monitoring of the load-deflection curve and failure modes. Finite element simulations were also conducted for the tested samples and compared with the experimental results. Furthermore, the model was used to explore additional parameters, such as the effect of shear reinforcement spacing and hybrid longitudinal reinforcement configurations.

## EXPERIMENTAL STUDY

Three experimental testing groups were performed. The first group was performed to identify concrete brick material. The second group was performed to identify the equivalent mechanical properties of the brick and the grout together. In the third group, three-point bending tests were conducted on masonry beams reinforced by steel and CFRP rebar. In the following sections, the details of these tests will be detailed.

### Concrete brick specimen preparation

Bricks are prepared from concrete according to the mixing ratios mentioned in Tab. 1, and an average compressive strength of 25 MPa was obtained. Using Portland cement with a grade of 42.5N. As for the aggregate used, it is local crushed dolomite of size (5 mm) with a particle density of 2.64 g/cm<sup>3</sup> and water absorption of 3.19%. The fine aggregate is local siliceous sand with a bulk density of 1.578 g/cm<sup>3</sup>, a particle density of 2.67 g/cm<sup>3</sup>, a fineness modulus of 2.66, and a dry unit weight of 1.68 t/m<sup>3</sup>. The dolomite, water, and sand were mixed for three min, and after preparing the homogenous mix, it is poured into a wooden mold with dimensions 115 mm wide, 60 mm high, and 2110 mm long. In which the mold has been divided into ten connected parts, and every two parts have 10 mm between them, resulting in a brick size of 95 mm wide, 50 mm high, and 200 mm long. There were about 20 wooden molds in this study to simultaneously build the most significant number of bricks. The inner surfaces of each wooden mold were well-oiled before casting the concrete. The fresh concrete is cast in the molds in three layers, and each layer is compacted with a tamping rod. The bricks were left in the forms for 24 hours after the concrete pour was finished. Then the bricks were cured by submerging them in clean tap water for 28 days. Five hundred bricks were built and each brick was designed with two holes, and the diameter of one hole is about 35 mm to place the rebar inside. There are two different types of bricks in this experiment study, i.e., groove bricks and ordinary bricks, as shown in Fig. 1a to 1b. Groove bricks were used to put steel stirrups inside them. The groove size is 10 mm in width, 10 mm in height, and 200 mm in length.

Cement (kg/m <sup>3</sup> )	Coarse aggregate (kg/m <sup>3</sup> )	Fine aggregate (kg/m <sup>3</sup> )	Water (kg/m <sup>3</sup> )	W/C (%)	28-day compressive strength (MPa)
350	1100	700	210	60	25

Table 1: The weight ratios of concrete mix materials per cubic meter.

Two types of reinforcing rebar, i.e., hybrid steel/CFRP and CFRP rebar, were used in the experimental study. Reinforcing steel bars are a diameter of 4 mm, with a yield tensile strength of 400 MPa are used. The mechanical properties were conducted on three CFRP rebars tested in tension. Test results showed the significance of the CFRP rebar as reinforcement bars of diameter 4 mm, as shown in Tab. 2 and Fig. 2.

Specimen	Diameter (mm)	Yield Load(kN)	Yield strength (MPa)	Ultimate load(kN)	Tensile strength (MPa)	Tensile strain at ultimate load (%)	Tensile strain at yield load (%)	Elastic tensile modulus (GPa)
CFRP	4	-	-	20.095	1600	1.32	-	121
Steel	4	5.024	400	7.536	600	8.5	0.3	200

Table 2: Mechanical properties of steel and CFRP rebar.



Figure 1: Samples Casting; a) Casting brick samples, b) Bricks after curing, c) Concrete cubes, d) Masonry cube samples, e) Masonry prism samples.

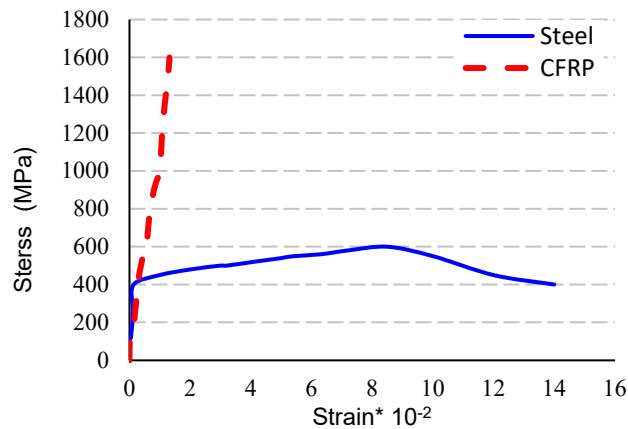


Figure 2: The stress-strain curve for reinforcement bars.

*Concrete compression strength tests*

Average compressive strength at 25 MPa was obtained by testing three concrete cubes with dimensions of 100 x 100 x 100 mm after 28 days, as shown in Tab. 3. A hydraulic testing machine of capacity 2000 kN and rate of loading  $0.30 \pm 0.05$  N/(mm<sup>2</sup>.s) is adopted for compressive strength. The compressive strength was calculated by average for three identical cubes by dividing the ultimate test failure load by the cross-section zone of the test specimens. A compression test is conducted according to BS 1881-116 [21]. Figs. 3a and 3e show the compressive strength test specimens and machine used for tests.

No of Specimens	Dimensions (mm)	Area (mm) <sup>2</sup>	Load (N)	Stress (MPa)	Strain (%)	Modulus of elasticity (MPa)
1	100x100x100	10000	250000	25	0.2385	10485
2			245000	24.5	0.2368	10345
3			253000	25.3	0.2371	10670
Average			249000	25	0.2375	10500

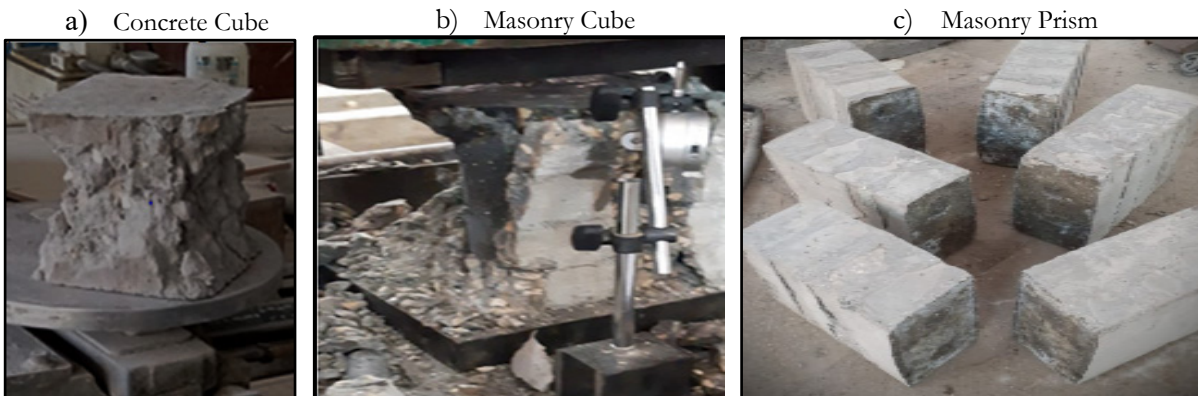
Table 3: Mechanical properties of concrete cube.

*Equivalent mechanical properties tests*

The compressive tests were carried out on six masonry cubes with dimensions of 200 x 200 x 200 mm after 28 days to determine the equivalent material's compressive strength and modulus of elasticity, as shown in Tab. 4. A hydraulic testing machine with a capacity of 1500 kN and a loading rate of 100 kN/sec is adopted for compressive strength. The compression strength ( $f_m$ ) was calculated by dividing the ultimate test failure load by the cross-section zone of the test specimens. Figs. 3b and 3d show the compressive strength test specimens and the stress-strain curve.

No of Specimens	Dimensions (mm)	Area (mm) <sup>2</sup>	Load (N)	Stress (MPa)	Strain (%)	Modulus of elasticity (MPa)
1	200 x 200 x 200	40000	950000	24	1.3660	1757
2			820000	20.5	1.4898	1376
3			750000	18.75	1.1890	1577
4			920000	23	1.2749	1804
5			840000	21	1.2331	1703
6			770000	19.25	1.0821	1779
Average			841667	21	1.2655	1666

Table 4: Mechanical properties of masonry cubes



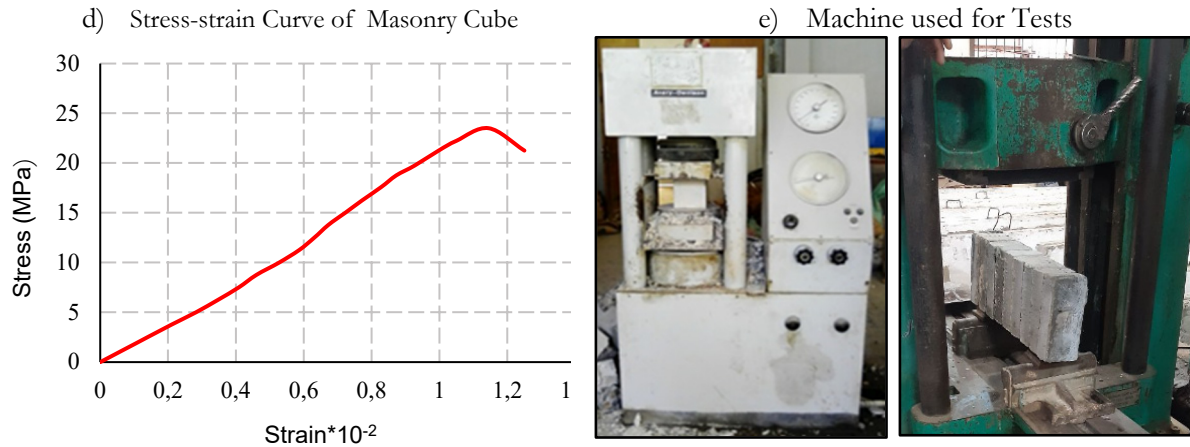


Figure 3: Samples Testing; a) Failure of Concrete Cubes, b) Failure of Masonry Cube, c) Failure of Masonry Prism, d) Stress-strain Curve, and e) Testing Machines.

Three-point bending tests were carried out on three masonry prisms with dimensions of 95 x 200 x 530 mm after 28 days. Figs 3c and 3e show the flexure strength test specimens and the machine used for tests. In this instance, the equivalent material's tensile strength is determined using Eqn. (1). These specimens had an average tensile strength of 1.78 MPa.

$$f_{tb} = \frac{3 * p * l}{2 * b * d^2} \quad (1)$$

where  $f_{tb}$  is the flexural strength in (MPa),  $p$  is the failure load in (kN),  $b$  is the breadth of the section in (mm),  $d$  is the effective depth in (mm), and  $l$  is the span from center to center in (mm).

### *Masonry beams' tests*

A bricklayer was used to conduct the specimens, considering the thickness of the mortar for all joints. Three beams were built using concrete bricks. Sika grout was used as the mortar between the bricks. Every beam was built of 16 blocks, and a thickness of 10 mm for grout between rows of bricks was used. The grade of the used grout is 214N, which was procured in bags weighing 25 kg. The bricks were stacked on a flat surface and closed with plywood on three sides only. Longitudinal rebar was placed inside the two holes, and steel stirrups were placed inside the groove. The same 214N grade Sika grout was used to fill the void around the rebar. The grout's first layer was placed to stack the second brick and fill the groove, and so on. This process continued until 16 bricks were placed and cured for 28 days with wet burlap bags. Eight steel stirrups were placed, divided into eight bricks out of 16 bricks, i.e., one steel stirrup for every other masonry brick, spaced at 120 mm (0.78d) in specimens CFRP reinforced beam with stirrups RMBB and hybrid reinforcements and steel stirrups RMBC. The lower longitudinal reinforcement for all beams had different ratios of (Ø4) CFRP bars and steel/CFRP hybrid reinforcement bars. The upper longitudinal reinforcement of all beams had the same compression of (1Ø4) CFRP. The upper and lower longitudinal reinforcements were spaced at 105 mm. All beams were tested and processed after 28 days to determine the load-carrying capacity and were tested for failure. The three-point loading procedure was performed in tests of beams using a hydraulic machine with a capacity of 1000 kN under a single concentrated load at midspan to apply static load. A displacement control test was performed with a speed of 5 mm/min.

Initially, the beam was adjusted on the testing machine with the proper clear span of 840 mm. The beams rested on roller supports. The load is applied to the load cell at one point, which is placed on top of the beam specimen at mid-span. Once the beam is centered, the potentiometric transducer is mounted under the mid-span of the beam to measure the vertical deflection. The loading process continues until the failure of the beam specimens. Fig 4a to 4e illustrate the reinforcement of the three beams and test setup. The RMBA and RMBB have the same ratio of longitudinal CFRP reinforcement, except that the RMBB sample contains steel stirrups. It is important to note that the ratio of the CFRP bar in the hybrid reinforcement was 2:1 for the steel bar.

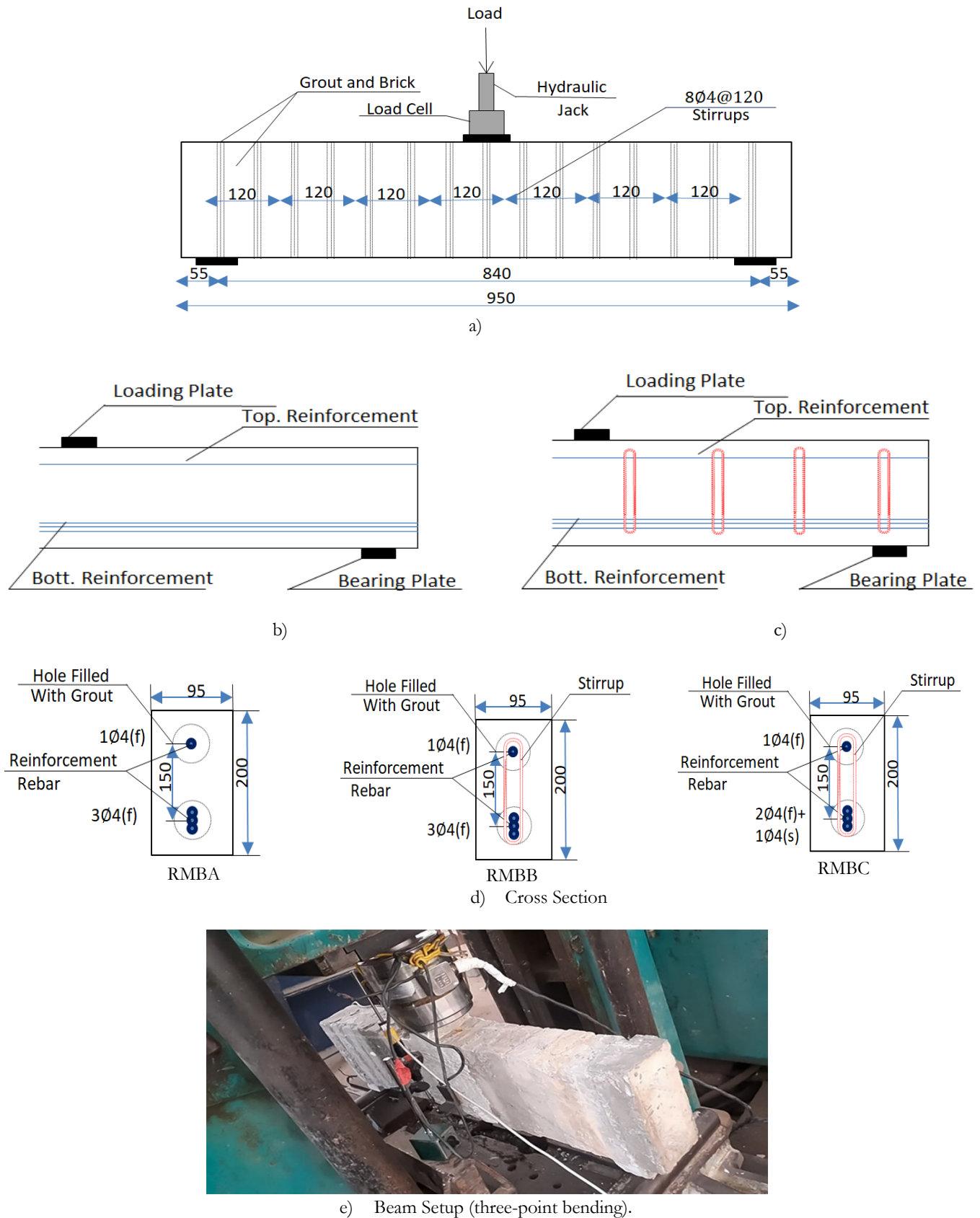


Figure 4: Geometric and Reinforcement details of beams; a) Beam side view, b) Side View of RMBA, c) Side view of RMBB and RMBC, d) Specimens cross sections, and e) Beam setup. (Dimensions in mm, the symbols "s" and "f" indicate steel and CFRP rebar, respectively).



## EXPERIMENTAL RESULTS AND DISCUSSION

In this section, the results obtained in the experimental study will be discussed for each specimen. The results include mode failure, cracking load ( $P_{cr}$ ), maximum load ( $P_m$ ), and their subsequent displacements ( $\Delta_{cr}$ ), ( $\Delta_m$ ) respectively. The summary of the results is found in Tab. 5.

Specimens	End of the first line elastic state		Maximum		Mode of failure
	Load (kN)	$\Delta_{cr}$ (mm)	Load (kN)	$\Delta_m$ (mm)	
RMBA	7	0.6	25	11.8	Shear
RMBB	8.8	0.93	25.7	6.14	Shear
RMBC	7	0.5	30.5	15.3	Flexure

Table 5: Results of testes beams.

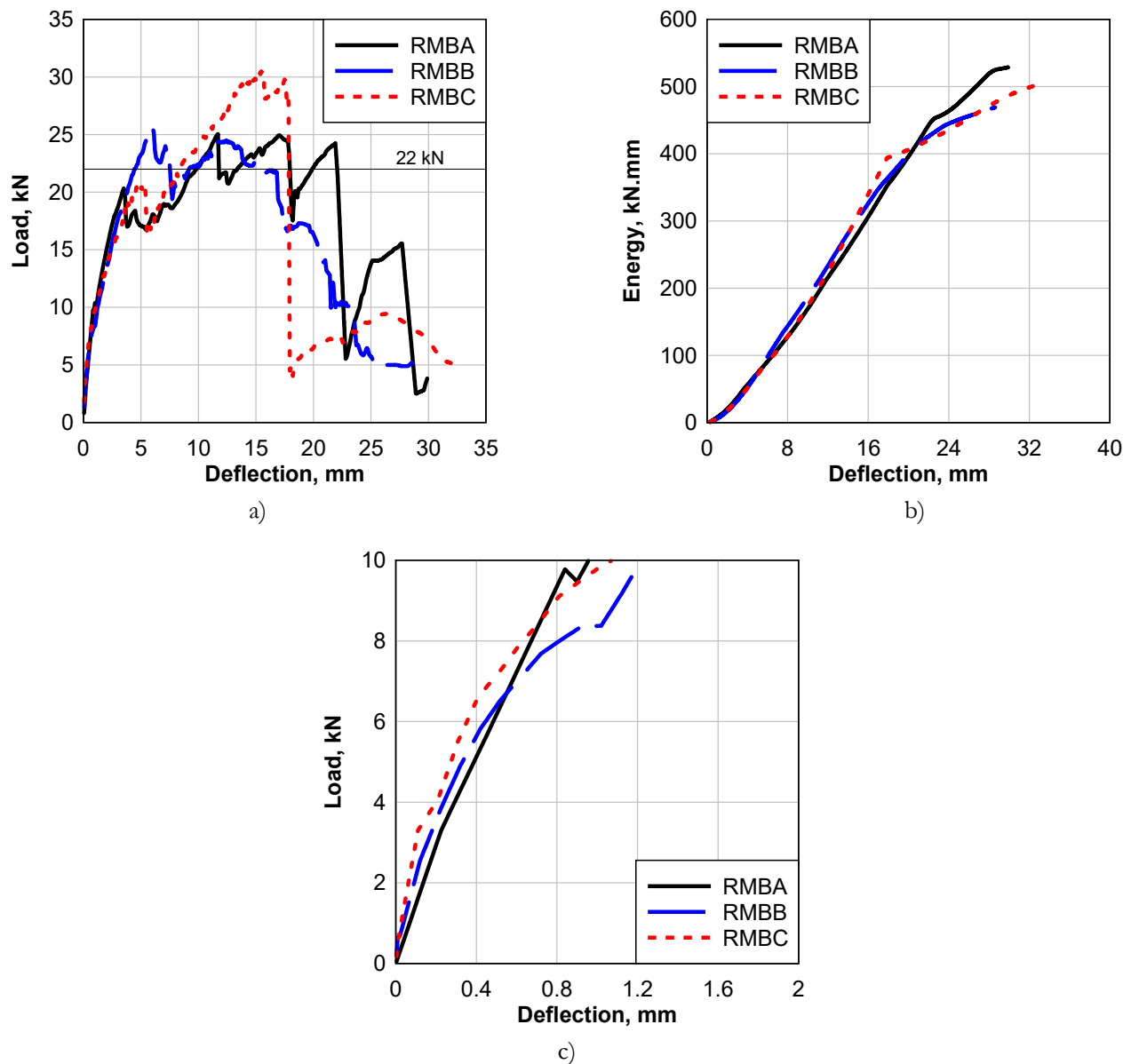


Figure 5: Experimental Results; a) Load vs displacement curves, b) Strain energy, and c) Zoom on the linear part of the curve.

### *Load-deflection curve*

Static three-point bending testing was evaluated to assess the ultimate capacity, load-deflection response, and failure modes. Fig. 5a represents the load-deflection curves evaluated from experimental tests of the beams. All the specimens have similar load-deflection behaviors. The load-deflection relationship consists of five stages. The first stage is linear and ends at the first cracking load. At this point, the tension side of the masonry developed tension cracks. The cracking load was identified by visual monitoring of the sample and the load-deformation curve. The first crack in the specimen RMBA occurred at a load of 7 kN with a corresponding deflection of 0.6 mm. However, in the specimen RMBC, the first crack appeared at the same load with a higher corresponding deflection of 0.5 mm. In specimen RMBB, the first crack appeared at 8.8 kN with a higher corresponding deflection of 0.93 mm than other experimental beams. The initial stiffness load was evaluated by interpolating the first part of the curve. The values for beams RMBA, RMBB, and RMBC, were 14.5 kN/mm, 16.68 kN/mm, and 24.34 kN/mm, respectively. Comparing samples RMBA and RMBB, shows that the shear reinforcement has a minimal effect on the initial stiffness. However, comparing RMBB and RMBC, shows that using steel increased the initial stiffness by 50%. It is worth mentioning that, although these values are in a logical order, they might be affected by the noise of the data acquisition system, as the displacement values are very small.

Thus, it can be concluded that the beam RMBA had the highest initial stiffness and lowest deflection, in contrast to the beam RMBB. After that, a nonlinear hardening stage continued and ended at 20.4, 25.7, and 20.8 kN for beams RMBA, RMBB, and RMBC, respectively. This point represents the first peak in the load-deflection relationship. After this point, the strength of the beams dropped by about 17, 25, and 22 % for beams RMBA, RMBB, and RMBC, respectively.

After this drop, the load increased again in RMBB and RMBC to reach a maximum value of 25.7 and 30.5 kN, respectively, while for RMBA, the first peak gave the maximum load.

At this point, the compression side of the masonry beam was subjected to crushing. Finally, after the maximum peak, a progressive softening failure was observed for all beams. It can be concluded that the maximum load of the specimen RMBB increased by only 3% compared to the beam RMBA due to the use of shear reinforcement. This indicates that the steel stirrups (0.78d) do not significantly affect the ultimate load. The beam RMBC achieved a higher load-carrying capacity than the other models. It was about 19% higher than the beam RMBB and 22% higher than the beam sample RMBA due to the use of hybrid reinforcement. At a load of 22 kN, the deflection for RMBA, RMBB, and RMBC was 9.8 mm, 4.6 mm, and 8.3 mm, respectively. This indicates that beam RMBB had the highest stiffness compared to other beams after cracking. The ability of the system to absorb strain energy reflects its performance under dynamic loads such as blasts and earthquakes. The strain energy was calculated by finding the cumulative area under the stress-strain curve. It can be observed that although RMBC had the higher strength, it did not provide the maximum cumulative energy, because the strength significantly dropped after the peak. Fig. 5b shows the mid-span deflection vs the strain energy.

### *Crack pattern and failure modes*

Fig. 6 illustrates the experimental patterns for beam specimens. Initially, the beam RMBA suffered from one flexural crack and two diagonal cracks originating from each side of the beam. As the load increased, two diagonal cracks widened from each side of the beam until the shear failure happened at 25 kN with a deflection equal to 11.8 mm. For the beam RMBB, one flexural crack at the mid-span had occurred perpendicular to the beam center line. Then a single diagonal crack originated on one side of the beam until failure happened at 25.7 kN with a deflection equal to 6.14 mm. The beams RMBA and RMBB experienced shear failure mostly in the grout joint. Thus, it can be concluded that the beam RMBA showed the shape of the diagonal cracks more clearly than the RMBB before failure.

The shear failure in RMBA happened due to the lack of shear reinforcements, however, for RMBB the shear reinforcement combined with the 100% FRP longitudinal reinforcement did not enhance the shear strength.

The beam RMBC exhibited flexural failure, and three vertical flexure cracks propagated at the mid-span. The existence of steel rebar enhanced the shear strength. As the load increased, two flexural cracks widened until failure occurred in the grout joint at 30.5 kN with a deflection equal to 15.3 mm. All beams failed due to CFRP rebar cutting; CFRP cutting began at the final stage of loading before failure.



(a)

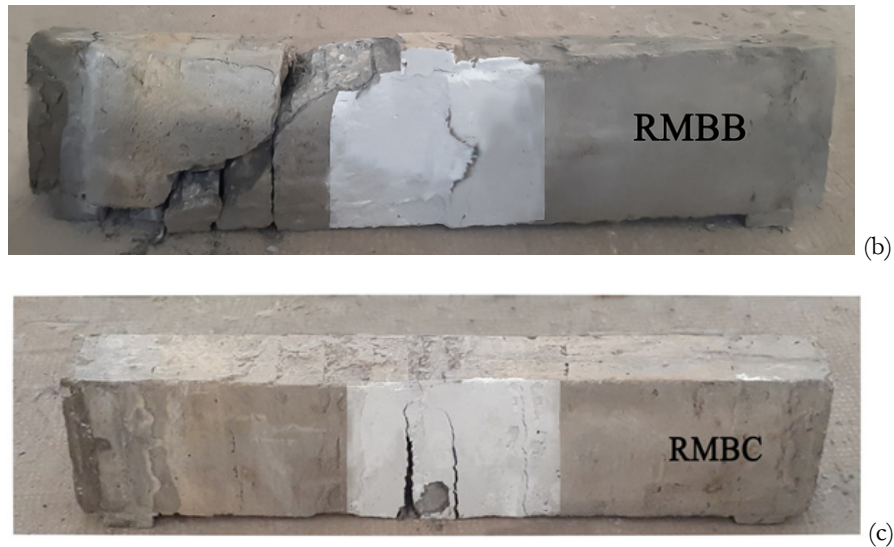


Figure 6: Crack patterns from experimental Beams.

### FINITE ELEMENT MODELLING

The material model used for concrete bricks is associated with the element SOLID 65. The model is defined by the concrete compressive strength, tension strength, shear stiffness for opened and closed concrete cracks, and residual stiffness after failure. This model simulates the elastic damage of concrete, but it can also include the effect of plasticity by adding multilinear isotropic hardening in relation to the material definition. At each element integration point, if the compressive failure criteria are achieved, the element loses its stiffness contribution at this point. The bilinear isotropic hardening plasticity model was used for the steel. This model's characteristics are the elastic characteristic, the yield stress, and the plastic tangent modulus. The mechanical properties were obtained from experimental work shown in Tab. 6.

Material	Property	Notation	Value	
Masonry	Elastic modulus	$E_m$	1666 MPa	
	Poisson's ratio	$\nu_m$	0.2	
	Compressive strength	$f_{mc}$	21 MPa	
	Tensile strength	$f_{mt}$	1.78 MPa	
Steel rebar	Elastic modulus	$E_s$	200 GPa	
	Poisson's ratio	$\nu_s$	0.3	
	Yield strength	$f_y$	Longitudinal 400 MPa	Stirrup 240 MPa
CFRP	Elastic modulus	$E_f$	121 GPa	

Table 6: Mechanical properties of masonry, steel and CFRP rebar.

An ANSYS parametric design language (APDL) code was used to input the material properties including the nonlinear stage of the stress-strain curve by processing commands. A numerical simulation was conducted to model only half beams with the same dimensions as those experimentally tested (95 x 200 x 950)mm to verify the tested beams' experimental findings Fig. 8. A three-dimensional (3D) Finite Element Model (FEM) was constructed by ANSYS 2020R20. The built FE model is made up of three distinct sorts of elements. A SOLID65 element was used to represent concrete components by 3D 8-noded solid elements with 3 degrees of freedom at one point by x, y, and z directions used to simulate masonry as concrete.

A LINK 180 element was used to model the steel CFRP reinforcement. Generally, steel is very uniform, unlike concrete, and the specification of a single stress-strain relation is satisfactory to be defined numerically. LINK180 was a uniaxial tension-compression characteristic so using this element is possible to represent trusses, cables, etc. The solid element SOLID 185 was used to model the loading and bearing plates [22][23]. Fig. 7 shows the components of the FE beam model. Masonry as concrete is attached to rigid steel plates by node merge. After performing, a convergence study, the model's meshed dimension was 15 X 15 mm [24–27].

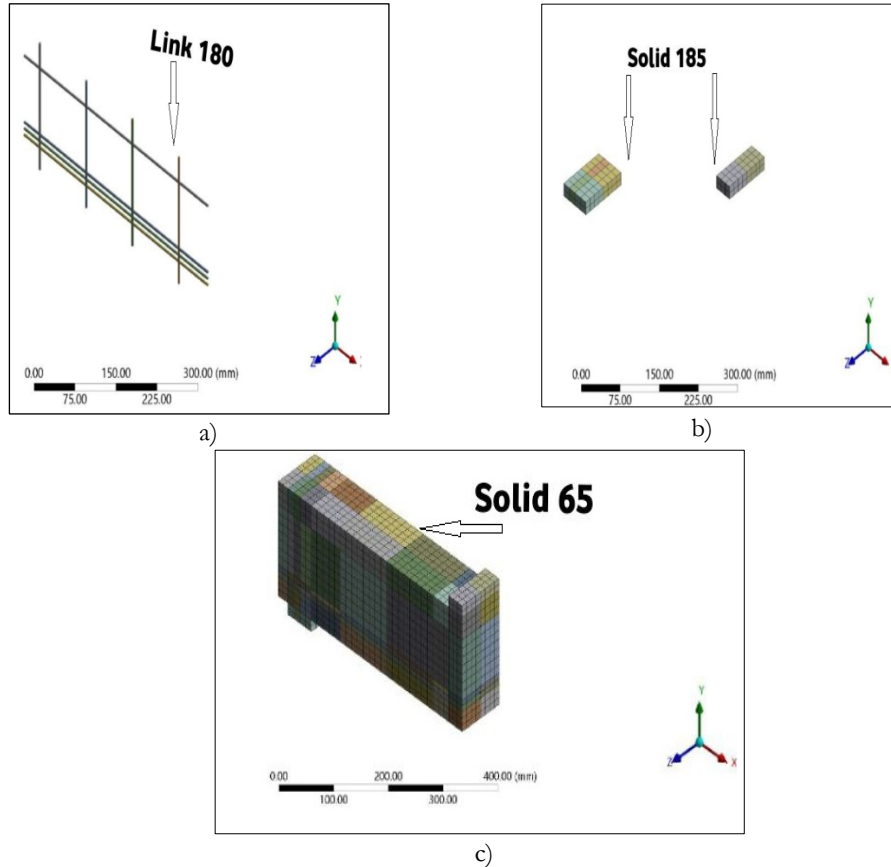


Figure 7: Components of the FE beam model; a) Reinforcement Rebar, b) Bearing Plates, and c) FE Mesh.

## COMPARISON BETWEEN NUMERICAL WITH EXPERIMENTAL

**F**igs. (8a, b, and c) and (9a, b, and c) show a comparison between the load vs displacement and crack patterns of the numerical model and the experimental tests. No difference was observed between the first cracks of all numerical beams compared to the experimental beams. Results revealed that the use of an equivalent material could simulate the behavior of masonry beams under static three-point bending, as shown in Figs. 8a, b, and c. Thus, it can be concluded that the numerical model accurately predicted the experimental results. Additionally, Tab. 7 revealed that the numerical could reasonably predict the maximum beam capacity with an average ratio (PFEM/PE<sub>exp</sub>) of 1.002 and a COV of 0.098. The initial stiffness load occurred at 10kN/mm and 7kN/mm for RMBA and RMBC, which are 43% and 50% of the value obtained in the experiment.

The mode failure of the three half models is shown in Figs. 9a, b, and c for beam RMBA, RMBB, and RMBC, respectively. As expected, the maximum deformation is found at the mid-span. In addition, for the beam without stirrups, shear failure significantly appeared near the support of the beam.

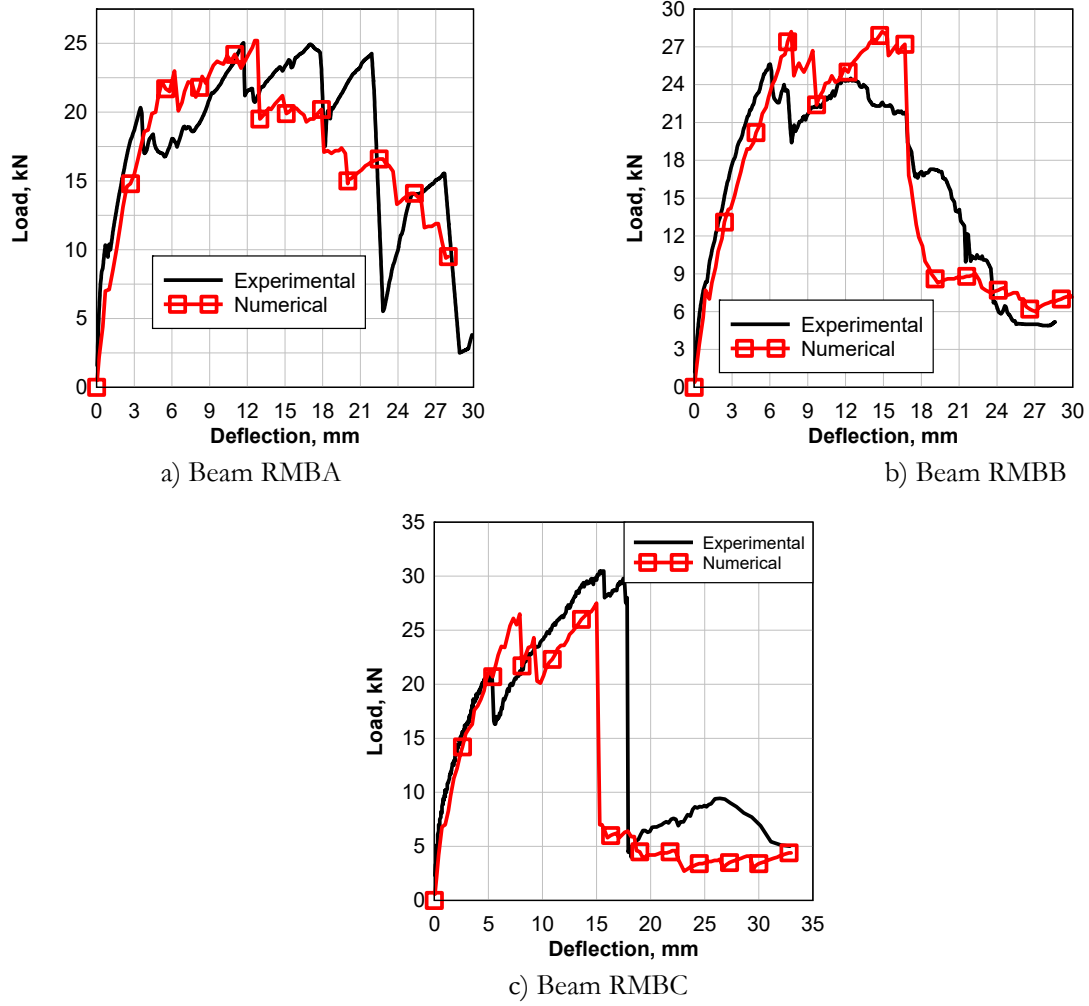
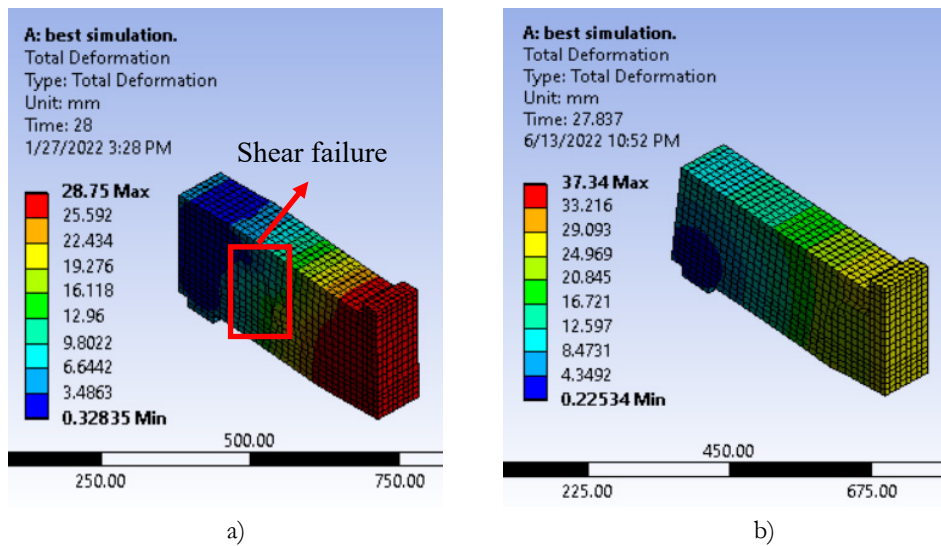


Figure 8: Comparison between the Experimental and Numerical Results; a) RMBA, b) RMBB, and c) RMBC.



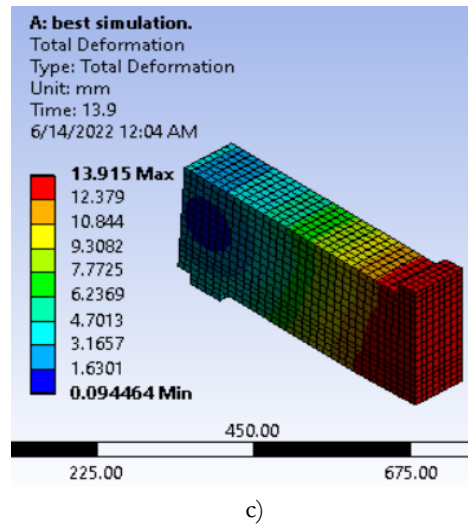


Figure 9: Investigation of mode failure Numerical beams: a) beam RMBA, b) beam RMBA and c) beam RMBC.

No	Experimental		Numerical		$P_{num}/P_{exp}$	$\Delta_{num}/\Delta_{exp}$
	$P_{exp}$ (kN)	$\Delta_{exp}$ (mm) at max load	$P_{num}$ (kN)	$\Delta_{num}$ (mm) at max load		
RMBA	25	11.8	25	12.8	1.0	1.08
RMBB	25.7	6.14	28.2	7.7	1.09	1.25
RMBC	30.5	15.3	27.5	15	0.9	0.98
Mean					1.002	1.106
Coefficient of variation (COV)					0.098	0.125

Table 7: Summary of the experimental and numerical results.

### Effect of Shear Reinforcement

The validated finite element model was used to study the effect of shear reinforcement spacing on the beam behavior. Fig. 10a illustrates the load-deflection curve for the beam RMBB with various shear reinforcement arrangements. Three models were studied and compared. In the first model (RMBB-60), the stirrups were placed on every masonry block at a spacing of 60 mm (0.39d). In the second model (RMBB-120) (The same results of RMBB), the stirrups were placed every 2 blocks at a spacing of 120 mm (0.78d); however, in the third model (RMBB-NO) (The same results of RMBA), there were no stirrups. The results of model RMBB-NO and RMBB-120 in Fig. 10a are the results of Figs. 8a and b, respectively; in this section, we changed the name to easily compare the results.

Before the first peak, no significant difference was observed in the load-deflection relation as the masonry section is working in both tension and compression zones. The first peak happened at 29.425, 28.2, and 22.2 kN of the models RMBB-60, RMBB-120, and RMBB-NO, respectively.

It can be observed that increasing the number of stirrups in RMBB-60 case, enhanced the ultimate shear failure by 6 and 19% compare to the cased RMBB-120 and RMBB-NO, respectively, due to the increase in shear strength. After the first peak, the model RMBB-60 had the ultimate load of 29.93 kN. Results revealed that using shear reinforcement with a spacing of 0.78d at RMBB-120 increase the shear capacity of the tested beam with only 12%. Fig. 10b shows the mid-span deflection vs the strain energy, it can be seen that (RMBB-NO) had the maximum total strain energy, and no significant difference between (RMBB-60) and (RMBB-120) was observed. The mode failure of the three half models is shown in Fig. 11a to 11b for beams RMBB-120 and RMBB-60.

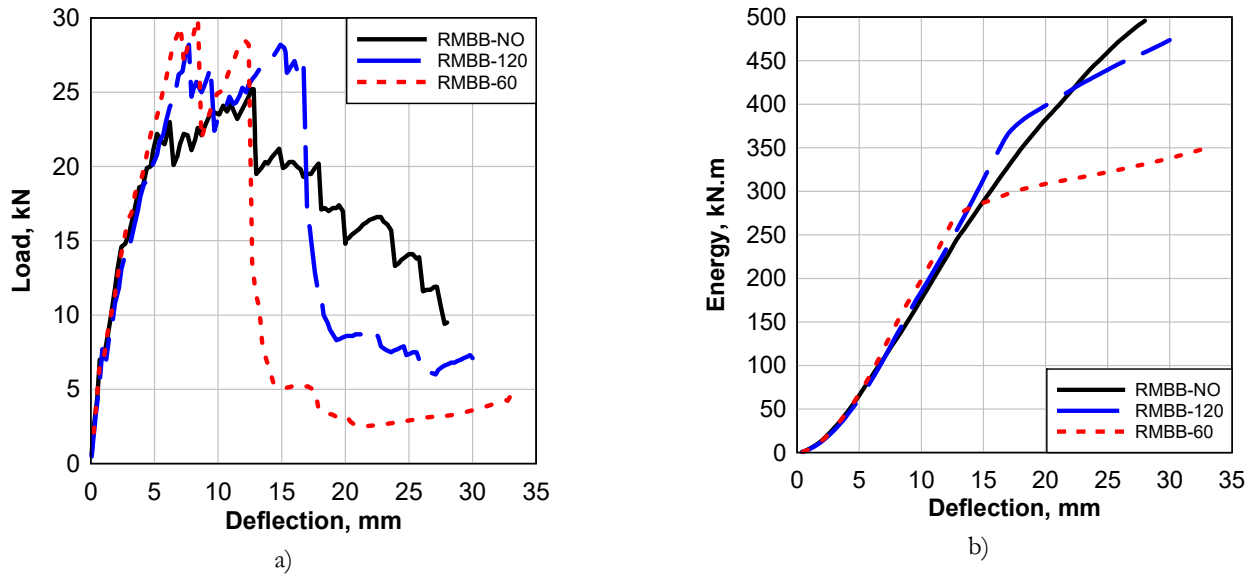


Figure 10: Effect of Stirrup Arrangements; a) Load vs displacement curves and b) Strain energy.

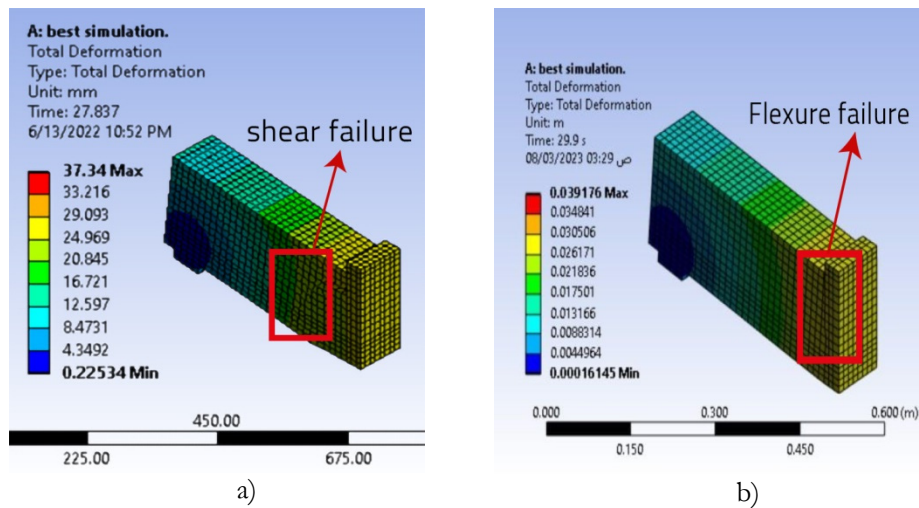


Figure 11: Investigation of mode failure Numerical beams: a) beam RMBB-120, and b) beam RMBB-60.

### Effect of CFRP Reinforcement ration

Fig. 12a illustrates the load-deflection curve for the sample RMBC with various hybrid CFRP/steel tension reinforcement combinations. Four models were studied numerically and compared; all four models had the same compression of (1Ø4) CFRP. In the first model (RMBC-2f1s), 2 CFRP rebar and one steel rebar were used. In the second model (RMBC-2s1f), 2 steel rebar and one CFRP rebar were used. In the models, RMBC-3s and RMBC-3f, three steel and CFRP rebar were used, respectively. The hybrid CFRP/steel rebar combination significantly affected the beam behavior. The best reinforcement combination was in the model RMBC-2f1s which has 2 CFRP rebar and 1 steel rebar (CFRP/steel=2).

For the RMBC-3f model, the first peak has the maximum value among the three combinations. However, the second peak came at 13% less than the peak value of the RMBC-2f1s beam. As that, for the RMBC-3s model, the strength was about 50.8 % of the ultimate load of the RMBC-3f model. Thus, the pure steel reinforcement gave the lowest strength. It can be concluded that using hybrid reinforcement, with mostly CFRP rebar will give the best strength and ductility response. Fig. 12b shows the mid-span deflection vs the strain energy. The best total strain energy was in the model RMBC-2s1f which has 2 steel rebar and 1 CFRP rebar. The worst total strain energy was in the beam RMBC-3s which has 3 steel rebar.

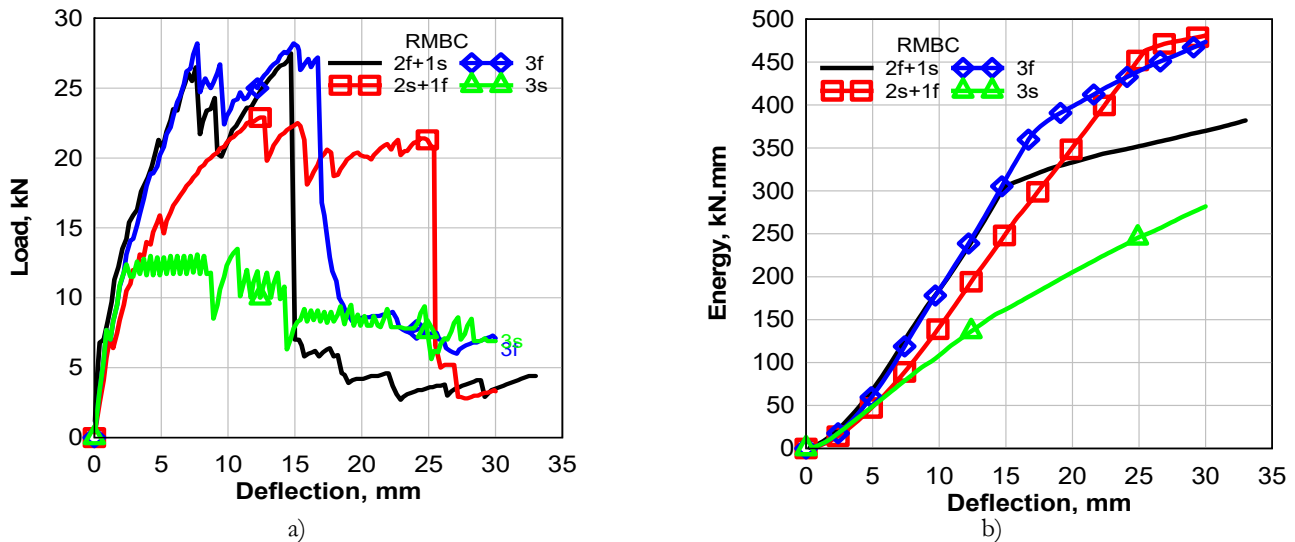


Figure 12: Effect of Stirrup Arrangements; a) Load vs displacement curves and b) Strain energy.

## CONCLUSIONS

The results of a tested and numerical study of reinforced beams subjected to three-point bending were presented. The study goal is to know the impact of CFRP reinforcement bars on beams and to evaluate the efficiency of numerical simulations using the equivalent brick properties. Three different experimental specimens with different longitudinal and shear reinforcements were developed. The results were used to understand the impact of reinforcement on the failure mode and the load-carrying capacity of the specimens. In addition, simulation models were created and validated using these experimental results. The following conclusions were reached based on the tested and numerical results:

- Experimental results showed that the beams with pure CFRP reinforcement whether it contains stirrups or not failed due to shear failure and the beam with hybrid reinforcement failed due to flexural failure.
- From experimental work; the hybrid steel/CFRP-reinforced beam with shear reinforcement achieved the highest capacity. It was about 19% higher than the CFRP-reinforced beam with shear reinforcement and 22% higher than the CFRP-reinforced beam without shear reinforcement.
- No enhancement in shear capacity for masonry beams with shear reinforcement with spacing 0.78d.
- It can be concluded that reinforcing the masonry beam can enhance both the shear and flexural performance of masonry construction.
- The numerical models with equivalent block properties could reasonably predict the maximum beam capacity with an average ratio ( $P_{num}/P_{exp}$ ) of 1.002 and a COV of 0.098.
- Shear reinforcement with 0.39d changed the mode of failure from brittle shear failure to ductile flexure failure.

## REFERENCES

- [1] Kara, I.F., Ashour, A.F., K rođlu, M.A. (2015). Flexural behavior of hybrid FRP/steel reinforced concrete beams, *Composite Structures*, 129, pp. 111–121, DOI: 10.1016/j.compstruct.2015.03.073.
- [2] Arockiasamy, M., Chidambaram, S., Amer, A., Shahawy, M. (2000). Time-dependent deformations of concrete beams reinforced with CFRP bars, *Composites Part B: Engineering*, 31(6–7), pp. 577–592, DOI: 10.1016/S1359-8368(99)00045-1.
- [3] Cousin, P., Hassan, M., Vijay, P. V., Robert, M., Benmokrane, B. (2019). Chemical resistance of carbon, basalt, and glass fibers used in FRP reinforcing bars, *Journal of Composite Materials*, 53(26–27), pp. 3651–3670, DOI: 10.1177/0021998319844306.
- [4] Amran, Y.H.M., Alyousef, R., Alabduljabbar, H., Alaskar, A., Alrshoudi, F. (2020). Properties and water penetration of structural concrete wrapped with CFRP, *Results in Engineering*, 5, DOI: 10.1016/j.rineng.2019.100094.



- [5] Pang, M., Dong, Y., Liu, X., Sun, W., Lou, T. (2022). Prediction of structural behavior of continuous reinforced concrete beams with hybrid CFRP-steel bars, *Materials*, 15(21), pp. 7542–7559, DOI: 10.3390/ma15217542.
- [6] Thongchom, C., Bui, L.V.H., Poonpan, N., Phudtisarigorn, N., Nguyen, P.T., Keawsawasvong, S., Mousa, S. (2023). Experimental and numerical investigation of steel- and GFRP-reinforced concrete beams subject to fire exposure, *Buildings*, 13(3), 609, pp. 1–19. DOI: 10.3390/buildings13030609.
- [7] Bakar, M.B.C., Muhammad Rashid, R.S., Amran, M., Saleh Jaafar, M., Vatin, N.I., Fediuk, R. (2022). Flexural strength of concrete beam reinforced with CFRP bars: A review, *Materials*, 15(3), pp. 59–72, DOI: 10.3390/ma15031144.
- [8] ACI, C. (2015). ACI440.1R-15 Guide for the design and construction of structural concrete reinforced with fiber-reinforced polymer (FRP) bars, 22.
- [9] Joyklad, P., Waqas, H.A., Hafeez, A., Ali, N., Ejaz, A., Hussain, Q., Khan, K., Sangthongtong, A., Saingam, P. (2023). Experimental investigations of cement clay interlocking brick masonry structures strengthened with CFRP and cement-sand mortar, *Infrastructures*, 8(3), pp. 59–74, DOI: 10.3390/infrastructures8030059.
- [10] Ortiz, J.D., Khedmatgozar Dolati, S.S., Malla, P., Nanni, A., Mehrabi, A. (2023). FRP-reinforced/strengthened concrete: state-of-the-art review on durability and mechanical effects., *Materials (Basel, Switzerland)*, 16(5), pp. 1990–2020, DOI: 10.3390/ma16051990.
- [11] Milani, G. (2010). FE homogenized limit analysis model for masonry strengthened by near surface bed joint FRP bars, *Composite Structures*, 92(2), pp. 330–338, DOI: 10.1016/j.compstruct.2009.08.004.
- [12] Galal, K., Enginsal, M. (2010). Flexural Behaviour of GFRP-Reinforced Concrete Masonry Beams, *Journal of Composites for Construction*, 15, pp. 21–31, DOI: 10.1061/(ASCE)CC.1943-5614.0000148.
- [13] Rovnak, M., Nguyen-Minh, L. (2011). Shear resistance of GFRP-reinforced concrete beams, *Magazine of Concrete Research*, 63, pp. 215–233, DOI: 10.1680/mac.9.00182.
- [14] Haach, V.G., Vasconcelos, G., Lourenço, P.B. (2010). Assessment of the flexural behavior of concrete block masonry beams, *Materials Science Forum*, 636–637, DOI: 10.4028/www.scientific.net/MSF.636-637.1313
- [15] Singh, S.B., Munjal, P. (2016). Flexural response of masonry beam strengthened with FRP rebars, *Mechanics and Computation*, (August 2017), pp. 1731–1736, DOI: 10.1201/9781315641645-286.
- [16] Singh, S.B., Munjal, P. (2016). Flexural behavior of reinforced masonry beams with ECC as bed joint, *International conference on advances in concrete technology, Materials & Construction Practices*, Goa, India, 1, pp. 16–21.
- [17] Munjal, P., Singh, S. (2017). Flexural response of reinforced masonry beams with cement mortar as bed joint. *Conference: 13th Canadian Masonry Symposium*, Halifax, CanadaAt: Halifax, Canada.
- [18] Husain, M., Zaghallal, M., El-Sisi, A.E.-D., Samy, S. (2022). A comprehensive review on unreinforced and reinforced masonry structures modeling strategies, *The Egyptian International Journal of Engineering Sciences and Technology*, 39(1), pp. 13–24, DOI: 10.21608/EIJEST.2022.116902.1126.
- [19] Jasiński, R., Grzyb, K. (2021). Comparison of masonry homogenization methods – macromodelling and micromodeling of walls behaviour made of autoclaved aerated concrete masonry units, *IOP conference series: Materials Science and Engineering*, 1203(2), pp. 22033–22043, DOI: 10.1088/1757-899x/1203/2/022033.
- [20] Kömürçü, S., Gedikli, A. (2019). Macro and micro modeling of the unreinforced masonry shear walls, 3, pp. 116–23.
- [21] BS 1881-127. (1990). Testing concrete, construction standard, 2(2), pp. 1–14.
- [22] Abdelmaksoud, M., Khushefati, W., Khedr, M., Sayed-Ahmed, E. (2016). Steel beams strengthened with prestressed CFRP laminate: Is there a need for laminate prestressing?, *Electronic Journal of Structural Engineering*, 16, pp. 53–62, DOI: 10.56748/ejse.16210.
- [23] Sayed-Ahmed, E., Abdelmaksoud, M., Khushefati, W., Khedr, M. (2015). Performance of steel beams strengthened with prestressed CFRP laminate, *Electronic Journal of Structural Engineering*, 15, pp. 60–9, DOI: 10.56748/ejse.15203.
- [24] ANSYS. (2013). Ansys mechanical APDL theory reference, ANSYS Inc, Release15.
- [25] Hawileh, R.A., Musto, H.A., Abdalla, J.A., Naser, M.Z. (2019). Finite element modeling of reinforced concrete beams externally strengthened in flexure with side-bonded FRP laminates, *Composites Part B: Engineering*, 173, pp. 106952-106964. DOI: 10.1016/j.compositesb.2019.106952.
- [26] Sarsam, K., Al – Bayati, N., Mohammed, A. (2017). Finite element analysis of porcelanite lightweight aggregate reinforced concrete deep beams strengthened by externally bonded carbon fiber strips, *Journal of Engineering of Sustainable Development*, 21(1), pp. 124–138.
- [27] Dere, Y., Dede, F.T. (2011). Nonlinear finite element analysis of an R/C frame under lateral loading, *Mathematical and Computational Applications*, 16(4), pp. 947–958, DOI: 10.3390/mca16040947.